ISEIS

Journal of Environmental Informatics 11(2) 103-122 (2008)

Journal of Environmental Informatics

www.iseis.org/jei

Spatial-Temporal Variability of Northern Hemisphere Sea Ice Concentrations and Concurrent Atmospheric Teleconnections

J. M. Piwowar[1,*] and C. P. Derksen[2]

[1]*Department of Geography, University of Regina, Regina SK, S4S 0A2, Canada*
[2]*Meteorological Service of Canada, 4905 Dufferin Street, Downsview ON, M3H 5T4, Canada*

Received 16 October 2006; revised 4 May 2007; accepted 1 January 2008; published online 30 May 2008

ABSTRACT. Because the Arctic is so integrally connected with the Earth's climate system, there is concern that the recent era of global warming has irreversibly altered the polar sea ice cover. This can have global consequences. However, we need to improve our knowledge of sea ice-atmosphere teleconnections if we are to increase our confidence in such climate change scenarios. In this paper, we apply the method of principal components analysis to twenty years of pentad-averaged Arctic sea ice concentration anomaly data derived from satellite observations to retrieve the most significant spatial and temporal patterns. We then linked these patterns to coincident 500 mb geopotential height (500Z) data. The strongest spatial-temporal ice concentration anomaly pattern over the 1980-1999 period was the phase-shifted anomalies between the Greenland and Barents Seas and the Labrador Sea and in Davis Strait. We found this pattern to be associated with strong low pressure anomalies over the North Atlantic and is significantly correlated with the large-scale atmospheric patterns of the North Atlantic Oscillation and El Niño. Other regions where spatially and temporally consistent patterns of anomalous ice concentrations were identified include the Beaufort Sea, on the Siberian side of the Arctic Basin, and the Sea of Okhotsk. We identify the atmospheric patterns coincident with these anomalies. We conclude that our approach of linking PCA results of ice anomaly data with highly loading 500Z patterns is an effective analysis method. We recommend that this study be extended to link full atmospheric PCA results with the sea ice pentads used here.

Keywords: arctic sea ice, climate change, North Atlantic Oscillation, principal components analysis, teleconnections

1. Introduction

The Earth's climate is changing. An analysis of temperature records shows that the Earth has warmed an average of 0.6 °C over the past 100 years (NRC, 2000). The warming is real and significant, though its intensity has varied from decade to decade, from region to region, and from season to season. Projections suggest that over the next century, further warming of 1 to 3.5 °C will occur (IPCC, 2001). This warming is expected to be amplified in northern regions. Over just the two decade period of the 1980s and 1990s, there was an overall decrease in Arctic sea ice extent of over 5% (Parkinson et al., 1999). Since then the Arctic ice cover has continued to recede: In 2002 the Northern Hemisphere ice cover reached a record minimum, 14% lower than the average conditions examined in this research (Serreze et al., 2003).

These changes in Arctic sea ice are especially significant because of the high albedo of the ice cover. Under "normal" sea ice conditions, most of the incoming solar radiation that the polar regions receive is reflected back into space. When the sea ice cover retreats, however, more low-albedo ocean is exposed to the incoming radiation, absorbing this energy. The ocean layers are thus heated setting up a positive feedback loop further enhancing the warming of the polar regions.

Since sea ice is so intimately linked with the oceanic system beneath it and the atmospheric system above, all efforts to monitor and describe changes in the sea ice cover ultimately help to identify changes in the global climate system. Unfortunately, the effects that changing sea ice covers have on the atmosphere and changing atmospheres have on sea ice covers are poorly understood. We address this shortcoming in this paper by identifying spatially and temporally significant ice concentration anomalies and link these to concurrent atmospheric patterns.

Our primary objective of this study is to derive a better understanding of the nature of the Arctic sea ice cover by isolating its spatial and temporal characteristics and relating these to contemporary atmospheric circulation patterns (i.e., those which occurred at the same time). Our intention is not to identify cause and affect relationships; rather, it is to provide observational evidence for the linkages between the ice and the global atmospheric system.

A secondary objective is to establish a benchmark of sea ice-atmospheric teleconnections that can be used to validate

* Corresponding author. Tel.: +1 306 5855273; fax: +1 306 58534815.
E-mail address: joe.piwowar@uregina.ca (J. M. Piwowar).

ISSN: 1726-2135 print/1684-8799 online
 doi:10.3808/jei.200800115

observed climate changes in the future. Following the accepted procedures for defining atmospheric climate normals – i.e., a thirty-year baseline with a decadal update period – we desire to create a baseline sea ice climatology. Although our time span is only twenty years (1980-1999), this period is defined by the available data record of consistent satellite observations. We propose that an update applied in 2009 will provide a more accurate and useful indicator of change than other studies that declare change based on just three or four years of anomalous conditions.

To direct our approach to this problem, we focus our attention on the following two research questions:

- What are the most significant spatial and temporal patterns of Arctic sea ice concentration anomalies over the period 1980-1999?
- Are unique atmospheric patterns associated with any of these significant ice patterns?

1.1. Environmental Change Analysis by Remote Sensing

Remote sensing is an important source of information for environmental monitoring, principally arising from an established record of global observations dating back more than thirty years. The consistent and numerical nature of satellite imagery facilitates the semi-automated detection of environmental changes across broad spatial and temporal scales. For example, the impacts of an ecological disaster (such as an oil spill or a volcanic eruption) are easily mapped by comparing data from remote sensing images acquired before and after the event. Such bi-temporal analyses are limited, however, to describing the end results of a change; they offer little information on the intervening temporal processes.

As the satellite image archive continues to grow, more research attention has been focused on a class of remote sensing image processing algorithms, called multitemporal- (for analyzing tens of images) and hypertemporal- (for analyzing hundreds of images) techniques (Piwowar, 1995; Coppin et al., 2004). The advantage of multitemporal or hypertemporal procedures is that they have the potential to quantify variability characteristics of the phenomenon under investigation, not just change results. A variety of these procedures have been developed, including ARMA Time Series Modelling (Piwowar and LeDrew, 2002), Temporal Mixture Analysis (Piwowar et al., 1997), and Principal Components Analysis (Eastman and Fulk, 1993; Piwowar and LeDrew, 1996; Millward et al., 2006), with each method extracting different statistical properties of the data. Principal Components Analysis (PCA), for example, is a procedure that efficiently identifies unique spatial and temporal patterns; however, it does not produce statistically significance forecasts.

In this research we applied the PCA method to identify the most significant ice concentration anomaly patterns in remote sensing imagery over a twenty-year period. These patterns are then linked with coincident atmospheric analyses and evaluated within the context of other components of the polar climate system and published reports. Of all the potential hypertemporal analysis procedures, PCA is particularly well suited to this task since it is a technique that highlights the strongest spatial and temporal signals in a hypertemporal image sequence.

2. Data

2.1. Sea Ice Concentration Data

Sea ice concentrations derived from passive microwave satellite imagery were obtained from the National Ice and Snow Data Centre (NSIDC) at the University of Colorado at Boulder. Ice concentrations were calculated from microwave brightness temperatures using the Bootstrap algorithm (Comiso et al., 1997). The Bootstrap algorithm produces a temporally consistent time series of sea ice concentrations intended for use as a baseline for future measurements (NSIDC, 2000).

The passive microwave brightness temperatures were originally collected by the Scanning Multichannel Microwave Radiometer (SMMR) and Special Sensor Microwave/Imager (SSM/I) sensors which were aboard the Nimbus-7 and DMSP series satellites.

Passive microwave ice concentration imagery is frequently distributed (and processed) as either daily or monthly averages. We determined that neither of these frequencies would be suitable to meet our objective of identifying correlations between significant ice and atmospheric anomalies: The daily data were found to be too susceptible to influences from short-term passing weather systems, while important synoptic-scale events were likely to be missed entirely in monthly averages. Consequently we grouped the daily images into 5-day, pentad, averages. This produced 73 pentads for each year and 1460 images for the entire period. Standardized ice concentration anomalies were calculated by subtracting each pentad from the twenty-year mean for that pentad and dividing by that pentad's twenty-year standard deviation.

2.2. Atmospheric Data

Atmospheric data were taken from the National Center for Environmental Prediction (NCEP, formerly NMC – National Meteorological Center) gridded data product available from NCAR (National Center for Atmospheric Research) (Jenne, 1970). These data were selected because of their high level of acceptance and use in the atmospheric research community, and their consistency with other models' output (e.g., Roads et al., 1995; Trenberth and Olson, 1988). Roads et al. (1995) caution, however, that problem may exist in the NCEP data at near surface levels and at the 12 UTC observation time. In light of this finding, only the 00 UTC data were retained for analysis.

Given the shifts in tropospheric circulation that are potentially driven by global change, we extracted the 500 mb geopotential heights (500Z) data for our study. This fits with our overall interested in revealing potential associations between ice anomalies and global teleconnection patterns.

A 21 by 25 point region was extracted from the NCEP grid approximately covering the same area as the ice concentration

data. Daily data from 00 UTC were averaged for the same pentads as the ice concentration anomalies, providing a corresponding time series of atmospheric data.

Additional climatic diagnostics were acquired from the University of Washington: monthly values of the Pacific Decadel Oscillation (PDO), and the Arctic Oscillation (AO). The PDO depicts the leading principal component of monthly sea surface temperature (SST) anomalies in the North Pacific (Mantua et al., 1997; Zhang et al., 1997). The positive phase of the PDO produces anomalously negative pressure, while the negative phase produces a ridge structure in the North Pacific which influences atmospheric airflow over continental North America (Bond and Harrison, 2000).

The AO describes the leading sea level pressure (SLP) pattern in the Northern Hemisphere. The primary centre of action is in the Arctic, with opposing anomalies in the mid-latitude Atlantic-European and Pacific sectors. The AO is highly correlated with the North Atlantic Oscillation (NAO), and there is some debate regarding which of these two patterns better summarizes the fundamental Northern Hemisphere SLP structure (e.g. Deser, 2000). Earlier studies have shown the NAO pattern to be the strongest contributor to low-frequency geopotential height variance in the Northern Hemisphere, appearing consistently in all months of the year (Barnston and Livezy, 1987; Wallace and Gutzler, 1981). It is composed of a dipole of anomalies, the first centered over Greenland, the second extending across the central latitudes of the North Atlantic, reaching from North America to Europe. The positive phase of the pattern indicates below normal height and pressure at the northern dipole, and above normal height and pressure at the mid-Atlantic centre. The negative phase is associated with the reverse of these anomalies. Monthly atmospheric teleconnection indices acquired from the U.S. National Oceanic and Atmospheric Administration (NOAA) include the NAO, allowing it to also be incorporated into this study.

3. Principal Components Analysis

Principal Components Analysis (PCA) is a mathematical technique that has been shown to be of notable value in the analysis of remotely sensed imagery (e.g., Fung and LeDrew, 1987; Jensen, 1986; Lillesand and Kiefer, 2000) and climatological data sets (e.g., Kutzbach, 1967; Sellers, 1968; Kelly et al., 1982). The main objective of a principal components analysis is to enhance the separability, hence discriminability, of elemental features in the original data. The PCA transformation is applied through a rotation of the original measurement space into a new axis set, called components. A key characteristic of the derived principal components is that they are uncorrelated with each other. Thus given a data set in which there is significant correlation between the variables (as is common in remote sensing image time series), a principal components analysis will create new channels which have no correlation between them. This removal of inter-variable correlation has the effect of concentrating the information content of the original data into fewer parameters or channels. The first principal component accounts for the most variance in the original data; each successive component accounts for a smaller amount of the variance than its predecessor. Higher components thus define more spatially and temporally localized anomalies although they are representative of less "information" from the source data and more "noise".

For each component generated from our image time series we created a component image and its corresponding loadings plot. The component images graphically show the spatial associations identified by each component. We show areas of strong association with the spatial pattern defined by the component in white; regions that have a strong inverse association with the pattern are shown in black; other areas of weaker association are given mid-grey tones.

Component loadings are derived from the eigenvectors calculated during the PCA procedure. The component loadings indicate the degree of correlation between that component and the original data. They are scaled between −1 and +1. A high positive loading means the spatial patterns identified by the component are very similar to the patterns present in the corresponding sea ice pentad. A negative loading indicates an inverse spatial pattern between the ice data and the component. A loading near zero means there is little similarity. When plotted against time, loadings can be interpreted as an indicator of the temporal persistence of that given spatial mode. Extremes in the component loadings (both positive and negative) can be used to identify the temporal intervals when the spatial pattern characterized by a given component (or it's inverse) is present in the time series data. It should be noted that it is the strength of a loading that determines its significance. The sign of a loading (positive or negative), however, is arbitrary: if you flip the polarity of a loadings plot and make a grey-scale inversion in the corresponding component image, the pattern is still the same (Wilkinson, 1989).

Thus when we interpret a principal component we look both at the component image to determine *where* the component is correlated with the original data and at the loadings plot to find out *when* the spatial pattern of that component was strongest.

4. Ice - Atmosphere Analysis

A principal components analysis (PCA) of the 1460-image standardized concentration anomaly time series was computed. An analysis of the eigenvalues produced by the PCA suggested that the first five components, explaining about 15% of the total variance in the series, were the most unique in the sequence. We recognize, however, that the higher components likely exhibit important ice anomaly characteristics as well and we recommend their inclusion in subsequent analyses. We include a detailed analysis of the first five components below.

4.1. Analysis Sequence

In our examination of the significant ice anomalies and their associated atmospheric patterns below, we followed a standard analysis sequence. For each principal component:

- The loadings plot is presented and reviewed for notable tem-

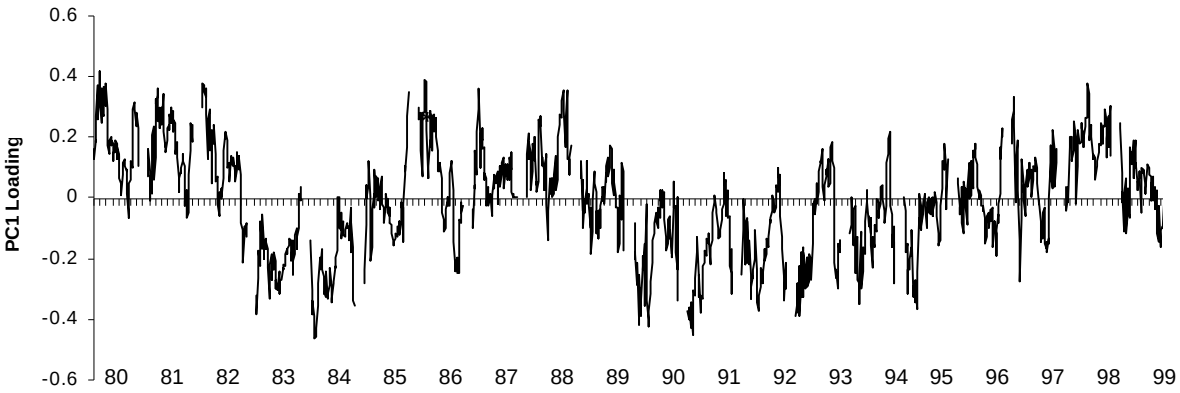

Figure 1. PC1 loadings.

poral patterns. Those pentads with loadings that are statistically significant at the 95% level are identified and marked on the loadings plot.

- A composite 500 mb geopotential height (500Z) map is computed by averaging the daily atmospheric fields for those dates of the statistically significant loadings. Separate 500Z composites are created for significant positive and significant negative loadings. The composite fields present the typical atmospheric conditions for intervals when the component ice pattern exists through the time series. Comparison of these average atmospheric fields will provide insight into whether unique atmospheric patterns are associated with any repeating modes of ice concentration anomalies.
- The component image is presented along with the 500Z composite just generated.
- The validity of the component image is verified. Note that PCA has the potential to generate numerically valid but physically meaningless components. Before evaluating each component, therefore, we look for consistent spatial patterns between the component image and actual ice anomaly images drawn from the satellite imagery. We consider a component to be valid if there is good spatial correspondence. If the patterns did not match, we would call the validity of the component into question. This situation did not arise during our analyses here.
- The validity of the 500Z composite pattern is verified. Since the atmospheric composites are mathematical constructs, we may be unsure about the spatial consistency of the average patterns they show. That is, "Are the composites good representations of the atmospheric patterns associated with the ice principal component?" One way to verify this is to perform a second principal components analysis (using a rotated varimax PCA for the atmospheric data to maximize the variance in each component) on the 500Z pentads used to generate each composite. If the atmospheric fields, which together created the group composites, are spatially consistent, the first within-group atmospheric component (*atmospheric sub-pattern*) should explain a majority of the variance within the dataset. The following hypothesis applies: the greater the similarity (therefore consistency) within each group, the greater the variance that will be explained by the first atmospheric sub-pattern. If the first atmospheric component explains a majority of the variance, then the pattern visualized by the composite image is relevant, and can be decisively linked to the component sea ice anomaly pattern. If multiple sub-patterns are needed to explain the majority of the variability within each atmospheric group, these various atmospheric sub-patterns need to explored further, and the group average must be discounted as physically irrelevant. These techniques are described more fully in Derksen et al. (2000).
- The 500Z sub-patterns are presented along with an indication of how well they represent their individual data fields. This is the lowest level of our analyses and is the basis for visually identifying ice-atmosphere relationships.
- The preceding steps are repeated for both positive ice anomaly loadings (*positive mode*) and negative loadings (*negative mode*).

4.2. Principal Component 1

Loadings for the first principal component (PC1) are plotted in Figure 1. The loadings show shifts between positive and negative modes on about a 3-year cycle prior to 1990. In the 1990s PC1 remained in a negative mode from 1990 to 1995 and recovered to weak positive peaks in 1997 and 1998. The highest positive mode occurred at the start of the series in January 1980 and PC1 was in its peak negative mode in February 1984.

4.2.1. PC1 Positive Mode

Figure 2a shows the first component image in its positive mode (PC1+). The strongest positive ice anomalies represented by this component occurred in the winter months. They are found in the Barents and Greenland Seas (in white), while the Davis Strait - Labrador Sea regions have negative anomalies (dark tones). There is also a weak positive anomaly present in the Sea of Okhotsk.

Principal components do not depict actual observable data patterns, but rather variance presumed to be evident in all

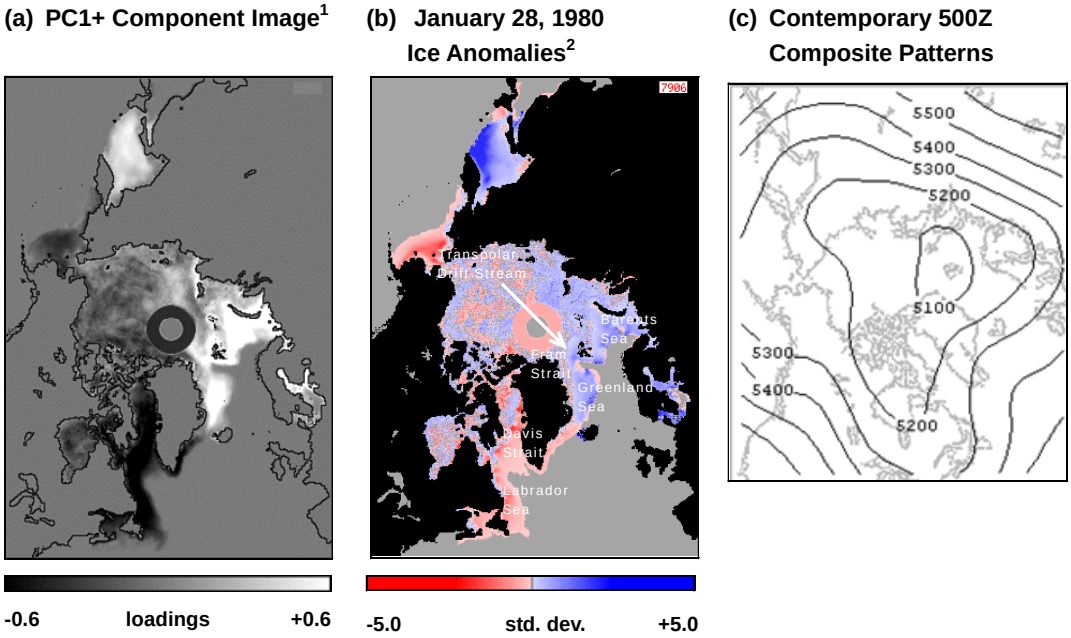

Notes: [1]White areas show strong association with the spatial pattern defined by this component; regions that have a strong inverse association with the pattern are shown in black. [2]Positive concentration anomalies (where there was more ice than the twenty year average) are shown in shades of blue; with the deepness of the hue proportional to the strength of the anomaly. Similarly, negative anomalies (where there was less ice than normal) are assigned varying shades of red, depending on the magnitude of the anomaly.

Figure 2. PC1+ image and composite 500Z patterns.

cases. In order to validate the spatial pattern presented in the component image we compare it with actual data from a highly loaded pentad. In Figure 2b the standardized ice concentration anomaly image for Pentad 7906 is presented. We see an excellent correspondence between the two images. Thus we conclude that the PC1+ component image is a useful synthesis of repeating spatial patterns in the hypertemporal series.

The strongest positive loadings observed in Figure 1 occur at the very start of the time series, in the winter of 1980. Parkinson and Cavalieri (1989) note that 1980 was the heaviest ice year for the Arctic as a whole between 1973 and 1987; this could be the result of large-scale wintertime ice divergence over large areas of the Arctic pack ice. Under cold and calm conditions, the newly formed inter-floe gaps would be quickly filled by new ice, thereby expanding the ice pack.

The 500Z Composite in Figure 2c was created by averaging all of the atmospheric pentads for the dates of significant positive ice anomaly loadings. The general pattern is of a weak low positioned over the eastern Arctic Ocean with some troughing over the Canadian Archipelago.

It should be noted, however, that the 500Z Composite image is a mathematical construct only. That is, even though it was created with 500Z pentads which all had strong loadings to the same ice component, those pentads may not have spatially similar patterns. In order to identify the consistency of the atmospheric composites, their atmospheric pentads were subjected to a rotated PCA to assess the within-group variability. The greater the similarity among the pentads, the greater the variance that will be explained by the leading atmospheric component and the greater the predictive potential of this analysis. The results of the atmospheric PCA for Ice Component 1 are summarized in Figure 3. The two leading components characterize the majority of variance in the data set, and therefore identify two alternative atmospheric modes that correspond to the positive phase of ice anomaly PC1. The $PC1+_1$ sub-pattern strongly resembles the complete group composite in Figure 2c with the main area of low pressure centered over the Arctic Basin and a smaller low pressure region over northern Hudson Bay. The cyclonic activity may be forcing more ice to move down the Transpolar Drift Stream towards Fram Strait, with some ice being diverted into the Barents Sea. This can be seen in the anomaly image of Figure 2b by generally higher than average ice concentrations over most of the Arctic Basin but strong positive ice anomalies in the Barents Sea, through Fram Strait, and into the Greenland Sea.

The second sub-pattern ($PC1+_2$) in Figure 3 characterizes an alternate mode of atmospheric circulation associated with the positive phase of ice anomaly PC1. The biggest differences between $PC1+_1$ and $PC1+_2$ are a shift in the location of the central Arctic low from the central Basin to the Greenland Sea in PC2 and a weakening in intensity. A center of high pressure over the East Siberian and Chukchi Seas is also evident

in PC1+$_2$. Cold winds blowing off the Asian land mass may be a contributing factor to the positive ice anomalies in the Sea of Okhotsk.

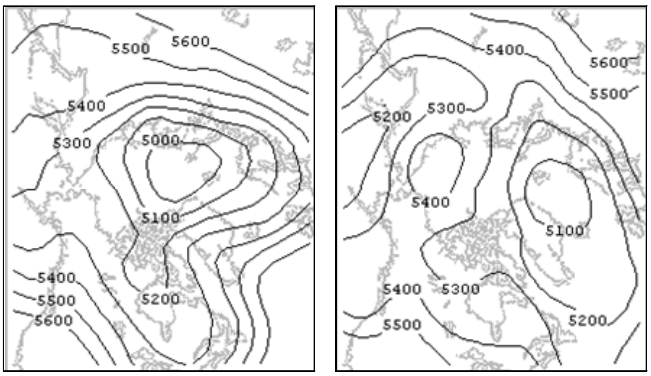

PC1+$_1$	PC1+$_2$
Variance Explained: 45%	Variance Explained: 30%
Representativeness:[1] 71%	Representativeness: 29%

Notes: [1]Representativeness is the percentage of 500Z fields that are most strongly loaded on this component.

Figure 3. PC1+ 500Z sub-patterns.

Another ice pattern observed in the PC1+ component image (Figure 2a) is the strong negative anomaly off the eastern North American coast. It is likely that under the eastern Arctic low pressure conditions of either PC1+$_1$ or PC1+$_2$ warm Atlantic air is pushed up through Davis Strait to reduce ice concentrations in Baffin Bay. This is especially evident in the PC1+$_1$ pattern which characterizes a ridge over southern Greenland and Davis Strait, allowing relatively warm air mass penetration from the North Atlantic.

4.2.2. PC1 Negative Mode

The strongest negative values in the PC1 loadings time series (PC1−) occurred in the winters of 1983 ~ 1984 and 1990 ~ 1993. The negative mode of a principal component represents a spatial reversal of the patterns observed in its positive condition. Consequently, the PC1− periods are characterized by increased ice concentrations from Baffin Bay to the Labrador Sea and less ice in the Greenland and Barents Seas, and in the Sea of Okotsk (Figure 4a). The similarity of the Pentad 8409 anomaly image in Figure 4b validates the component image.

The 500Z Composite image in Figure 4c shows a 500Z low pressure centre over Baffin Bay. The PCA decomposition of the PC1– atmospheric composite pattern revealed two complex sub-patterns (Figure 5). The first atmospheric sub-pattern (PC1–$_1$) exhibits a strong east-west pressure gradient extending across the Arctic Ocean from a High centered over the Kara and Laptev Seas to a Low pressure cell over the Beaufort Sea. There is also a weaker Low over the Greenland Sea. There are not any consistent nor strong ice anomalies in this region during these times, however, large, positive anomalies in Davis Strait and the Labrador Sea are characteristic.

In the second atmospheric sub-pattern (PC1–$_2$), the Beaufort Sea low has deepened and moved over the North Pole. There is generally low pressure over most of the Arctic Basin, the Canadian Archipelago, and along the eastern coast of Labrador. The Kara-Laptev high has strengthened and shifted to the east to hover over Northern Europe and Scandanavia. This has rotated the pressure gradient to be oriented north-south. These atmospheric patterns are associated with moderately positive ice anomalies in the Bering and Chukchi Seas as well as

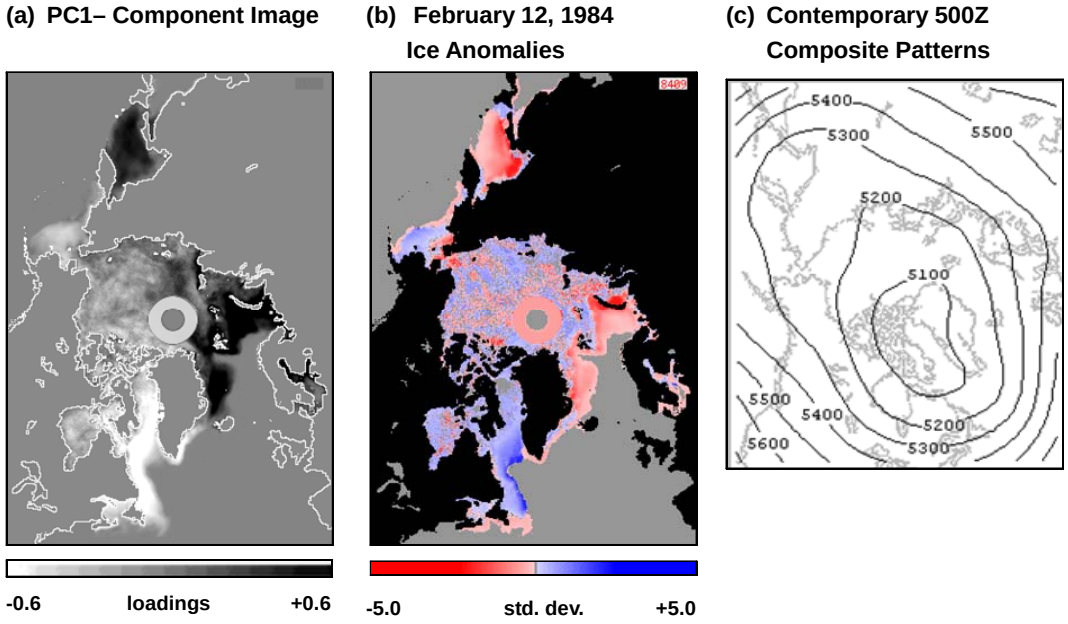

Figure 4. PC1– image and composite 500Z patterns.

increased iciness in Baffin and Hudson Bays.

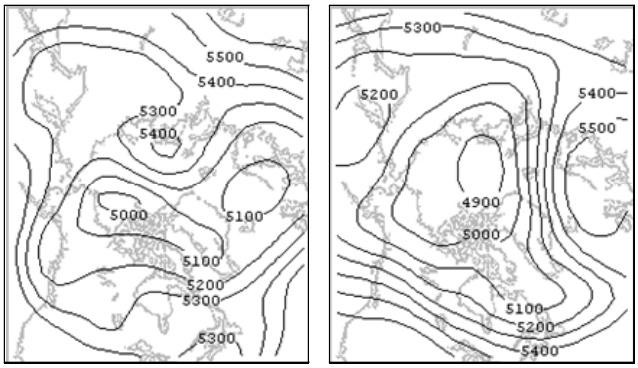

PC1–$_1$
Variance Explained: 37%
Representativeness: 53%

PC1–$_2$
Variance Explained: 24%
Representativeness: 32%

Figure 5. PC1- 500Z sub-patterns.

Colony and Thorndike (1984) found that the principal Arctic sea ice drift patterns, which arise from the general circulation of the atmosphere and ocean, clearly broke down in the 1983 to 1985 period. Thus a weakened Transpolar Drift Stream resulted in less ice being transported into the Barents and Greenland Seas, yielding lower concentrations in these regions. Heavy ice in the Labrador Sea region could also be oceanographically induced by means of a weaker West Greenland Current failing to keep the ice pushed further north, or it could be the result of the positioning and strength of the Icelandic low-pressure system, or both (Gloersen et al., 1993).

4.2.3. PC1 Analysis

We have identified two 500Z Composite patterns and four sub-patterns which have been found to occur repetitively from 1980 through 1999. These patterns are not evenly distributed across the observational time period, however. The positive modes are more prevalent in the 1980s while the negative modes dominate the early 1990s. There appears to be a strong spatial relationship between the positive mode of PC1 (PC1+) and low pressure centered over the eastern Arctic Basin (Figure 2). Conversely, when PC1 is in a negative mode (PC1–) the major low pressure centre shifts to locate over Baffin Bay /Davis Strait region. This is spatially coincident with the strong est negative values of PC1.

The PC1 phase-shifted ice anomalies between the Greenland and Barents Seas, in one mode, and Davis Strait and Labrador Sea, in the opposite mode, are likely connected to the large-scale atmospheric patterns of the NAO (Parkinson et al., 1999) and/or El Niño events (Piwowar and LeDrew, 1996). Over the time period we are studying here, the NAO has moved through three periods: a positive - negative oscillation prior to 1988; a prolonged NAO+ period between 1988 and 1996; and a dramatic reversal in phase in 1996 (Kwok, 2000). This description generally matches the PC1 loadings time series (Figure 1), except that a dramatic event is not apparent in 1996.

Alternatively, we know that there was a strong El Niño in 1983 ~ 1984, a weaker, but prolonged event from 1990 to 1995, and a very strong El Niño in 1988. Upon initial inspection, this sequence would appear to have even a better match with the PC1 loadings than the NAO. If the 1983 and 1990 events are related to PC1– modes (as the loadings would suggest), however, we cannot reconcile why the 1998 loadings are strongly positive.

To help understand the possible teleconnections we created monthly loading averages and correlated these with monthly values from the NAO, AO, and PDO. Weak, but statistically significant, time-lagged correlations were found between PC1 and the NAO and AO, peaking with the atmosphere leading the ice by one month (Figure 6).

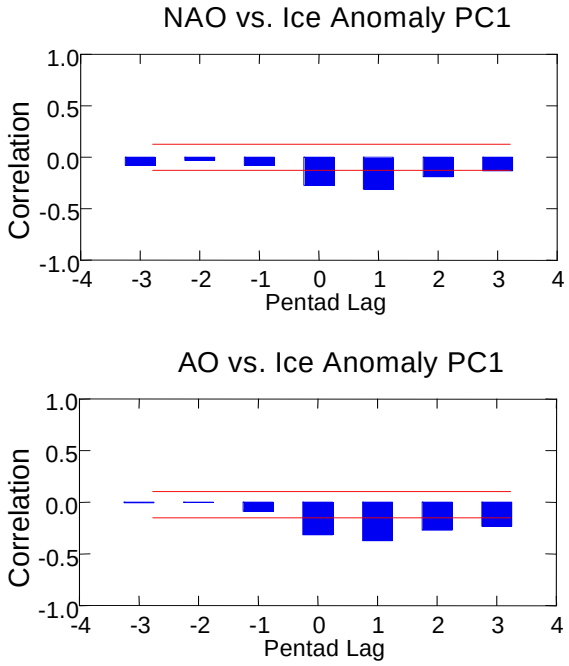

Figure 6. Lagged PC1-NAO and PC1-AO correlations.

4.3. Principal Component 2

Principal Component 2 (PC2) is generally negative from 1980 to 1988 and switches to a primarily positive mode for the remaining years (Figure 7). The lowest negative loading occurred in August 1985 and the most positive mode is found near the end of the time period in September 1998. PC2 is the seasonal inverse of PC1, with most of its significant loadings occurring between June and November.

4.3.1. PC2 Positive Mode

Principal Component 2 shows a broad region of negative concentration anomalies (dark areas in Figure 8a) across the top of North America. An example of a strongly loading ice anomaly for PC2+ (Pentad 9854) is shown in (Figure 8b). We

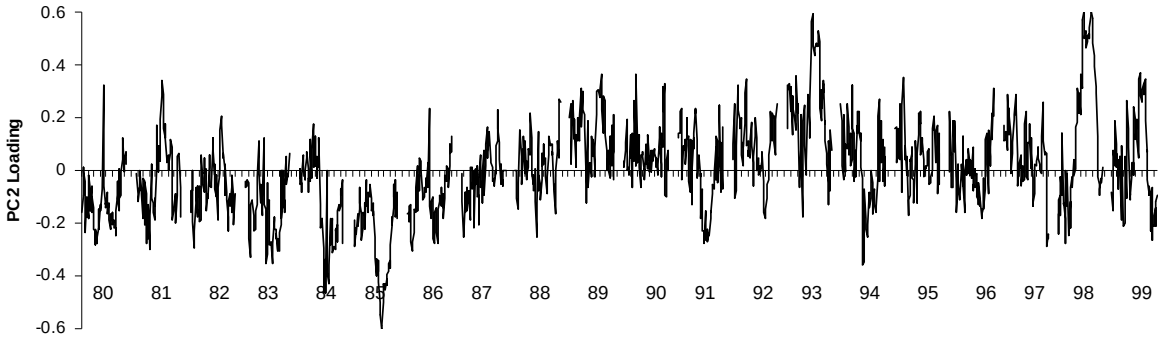

Figure 7. PC2 loadings.

see much lower than average ice concentrations across the Beaufort Sea and into the Canadian Archipelago. There are small positive ice anomalies in the Eurasian sector of the Arctic Ocean. The cyclonic activity associated with PC2+ is not as deep as the low pressure cells present during the sub-modes of PC1. Figure 9c shows the pressure distribution to be symmetrical about the pole with strong ridging over the Canadian Archipelago.

A PCA decomposition of the PC2+ atmospheric composite produced two significant sub-patterns: $PC2+_1$ dominates in the late spring and early fall ("cool" seasons), while $PC2+_2$ loads strongly during the summer months (Figure 9). $PC2+_2$ is especially dominant during the persistent anomaly event of July 1993. The lack of similarity between the 500Z sub-patterns and group composite for ice anomaly PC2+ indicates that the 500Z group composite in Figure 8c is likely not a significant pattern, but an average composed spatially unique patterns that are better characterized by the 500Z sub-patterns.

The cool season pattern in $PC2+_1$ is characterized by two Arctic lows over the Canadian Archipelago and the Barents/Kara Seas and is accompanied by moderately negative ice anomalies in the western Arctic Basin. Positive anomalies in Baffin Bay are also common at these times. The decrease in ice concentrations in the Beaufort Sea may be the result of the atmospheric forcing of the ice towards the pole. There does appear to be a build-up of ice around the polar data hole in the sample pentads presented in Figure 9.

The pattern in $PC2+_2$ is a typical warm season central polar low with a much weaker 500Z latitudinal gradient. The associated anomaly image (Figure 9b) shows an extensive area of significantly reduced ice throughout the western Arctic Basin. The extended duration of these ice anomalies (at least 15 days), time of year (late summer), and location (Beaufort Sea) suggests that this is an anomaly pattern associated with the quasi-annual reversal of the Beaufort Sea Gyre (LeDrew et al., 1991). The Beaufort Gyre is generally a counter-clockwise ro-

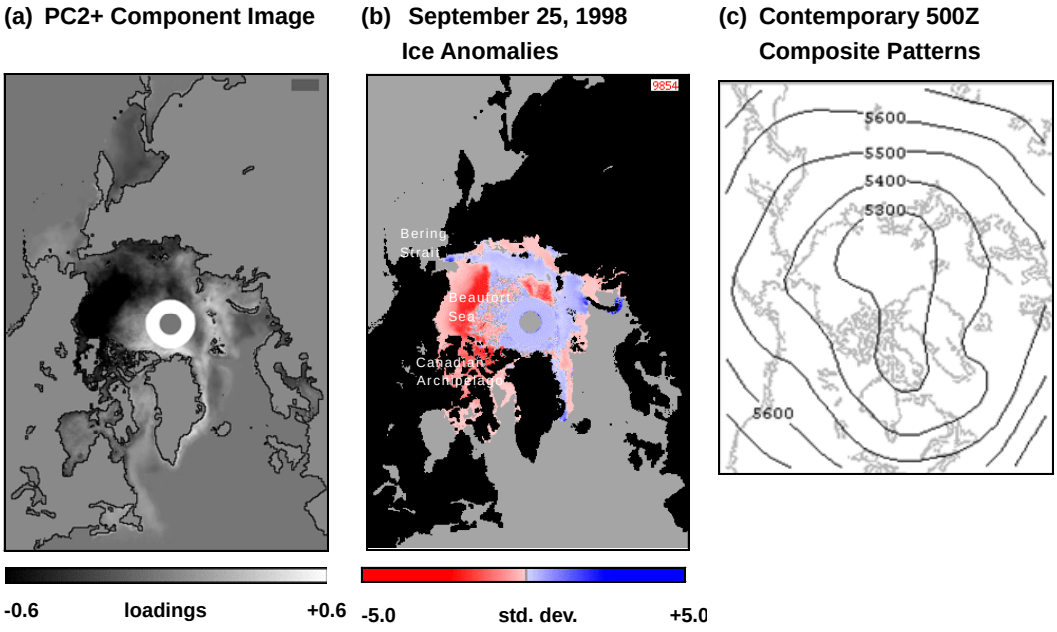

Figure 8. PC2+ image and composite 500Z patterns.

tational feature present in the Beaufort Sea and its ice cover. The gyre has been consistently observed to reverse its motion in late summer, possibly in response to a quasi-stationary low pressure system that locates in the area at this time (LeDrew et al., 1991). During the reversal periods there is divergence in the ice pack and an associated reduction in ice concentrations. Holt and Martin (2001) also suggest that northward flow of warm water through the Bering Strait contribute to these negative anomalies. Additional analyses of the ice anomaly images and contemporary PC2+$_2$ 500Z upper-air data would be required to confirm the Gyre-reversal hypothesis.

4.3.2. PC2 Negative Mode

The negative mode of PC2 shows strong increases in ice concentrations in the Beaufort Sea and Western Arctic Basin (Figure 10a). The anomaly patterns in Figure 10b are very consistent with the component image, thereby validating it. This mode was most prevalent in the 1980s, occurring for five temporally persistent events through the time series: August 1980, July/August 1983, July/August 1984, August 1985, and June/July 1994.

The atmospheric PCA decomposition shows that 2 components explain the majority of variance in the atmospheric data (Figure 11). Both of the PC2– sub-patterns characterize distinct low pressure systems north of Greenland and the Canadian Archipelago; the difference in orientation between these systems account for the two spatial modes. The low center in PC2–$_1$ is oriented from west to east as opposed to north to south in PC2–$_2$. A secondary PC2–$_2$ low pressure centre is located over the Aleutians which, when combined with strong ridging over western North America, forces the north – south orientation of the pattern in PC2–$_2$. The inverse relationship between 500Z pressure and latitude over the western Arctic Basin remains constant between both PC2– sub-patterns. Widespread positive ice anomalies occur in this region during the PC2– mode, perhaps induced by ice convergence toward the low pressure centre.

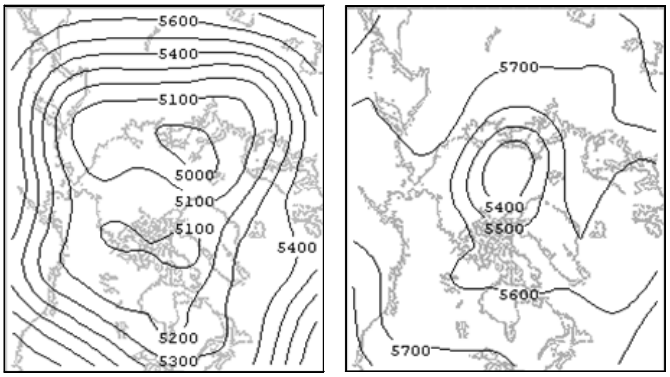

Figure 9. PC2+ 500Z sub-patterns.

4.3.3. PC2 Analysis

The second ice component is characterized by a regional anomaly centered over the western Arctic Basin. When in its positive mode, the anomaly is composed of reduced ice concentrations and increased iciness in this region is evident during PC2 negative modes. Both modes are associated with low pressure cells near the North Pole. PC2 is most likely to occur

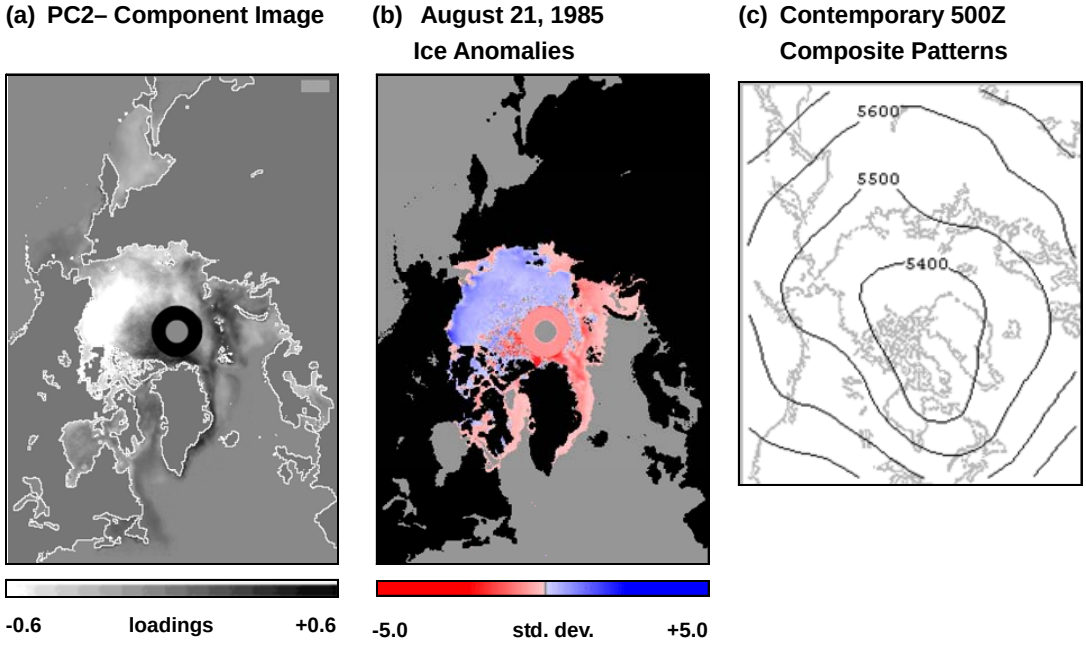

Figure 10. PC2– image and composite 500Z patterns.

during the warm months.

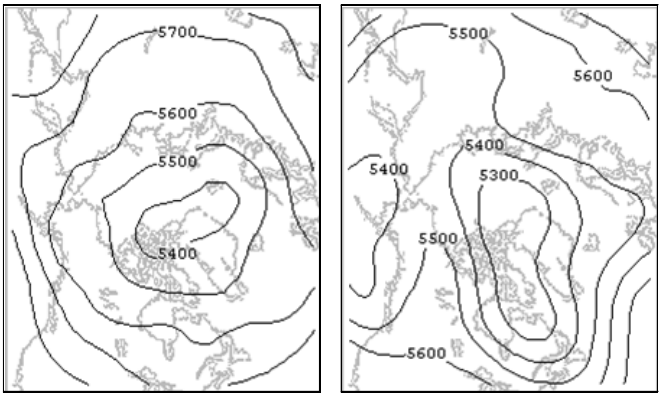

PC2–$_1$
Variance Explained: 45%
Representativeness: 67%

PC2–$_2$
Variance Explained: 31%
Representativeness: 33%

Figure 11. PC2– 500Z sub-patterns.

Interestingly, the positive and negative 500Z composites (Figure 8c and Figure 10c) are very similar to each other even though they are temporally associated with opposite phases of the same ice anomaly component. Upon closer examination, however, we note that, for both modes, the 500Z sub-patterns vary strongly from each other, and from the group composites. We question, therefore, the validity of the 500Z composites and wonder if there is one-to-many relationship between the atmosphere and this ice anomaly. It appears quite likely that several different 500Z pressure patterns are associated with the same general ice patterns.

We did not find any statistically significant lagged correlations between PC2 and any teleconnection time series.

4.4. Principal Component 3

Temporally, Principal Component 3 is largely inactive until 1989 when an extended negative mode began (Figure 12). Positive modes were dominant in 1992 to 1994 and again at the end of the series in 1998 and 1999. Visually, the loadings appear to oscillate between positive and negative modes in a 3-year cycle. A seasonal evaluation of the most significant loading pentads showed that although most of time the component is present in late spring/summer, there are some periods in December and January where the pattern reoccurs. This suggests the possibility of multiple atmospheric forcing patterns on the ice.

4.4.1. PC3 Positive Mode

This component shows strong anomalies in many of the peripheral seas ringing the Arctic Ocean (Figure 13a). In particular, the PC3+ image shows a strong positive loading in the East Siberian Sea. This pattern is not evident in the pentad with the highest positive loading, Pentad 9871 (Figure 13b), leading us to conclude that the positive mode image is a statistical fabrication. Consequently we did not analyze this component further.

4.4.2. PC3 Negative Mode

The negative mode of the third component shows positive ice anomalies in the Beaufort and Greenland Seas, as well as in Hudson Bay. These are balanced with a negative anomaly in the East Siberian Sea (Figure 14a). Pentad 9038 (Figure 14b), taken at the strongest negative loading, corresponds well with the component image. The 500Z composite (Figure 14c) shows a weak depression centered in the Arctic Ocean, just north of Greenland. The PC3– composite resembles the 500Z composites for ice PC1 negative and ice PC2 negative, however, so the new insight provided by this composite is limited.

Two sub-patterns were derived from the PC3– atmospheric composite (Figure 15). The PC3–$_1$ sub-pattern shows a low

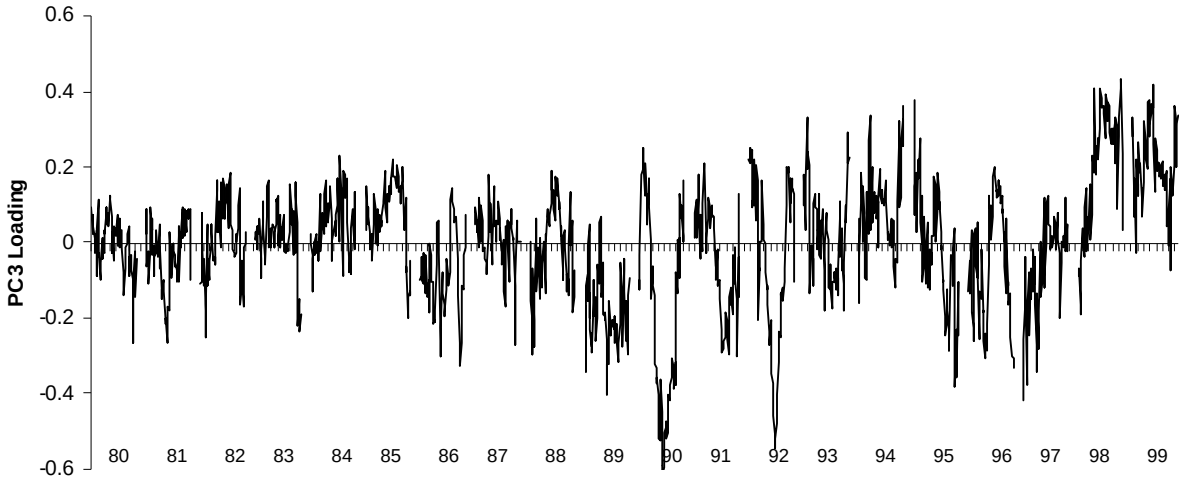

Figure 12. PC3 loadings.

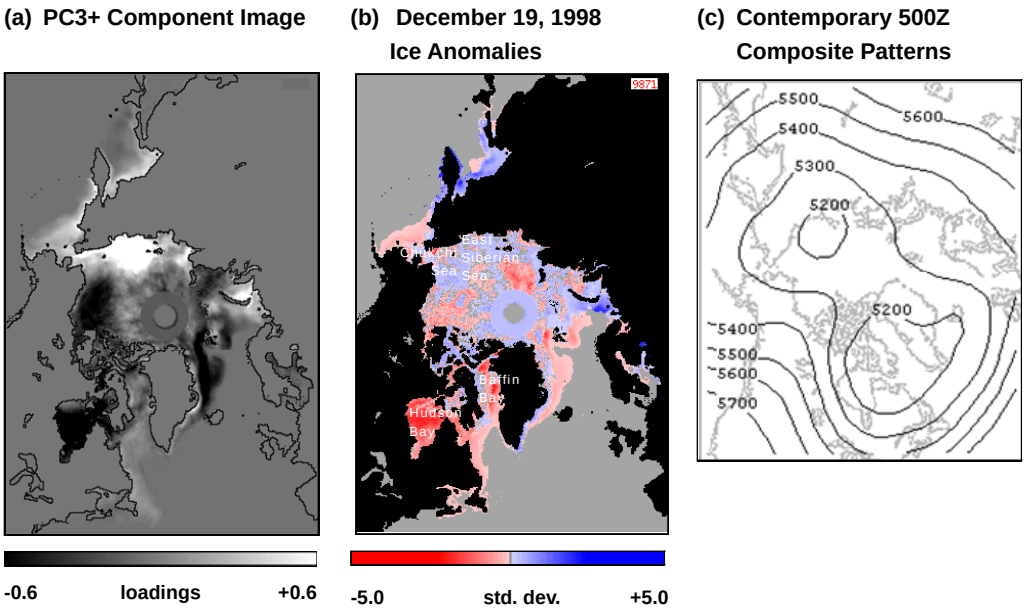

Figure 13. PC3+ image and composite 500Z patterns.

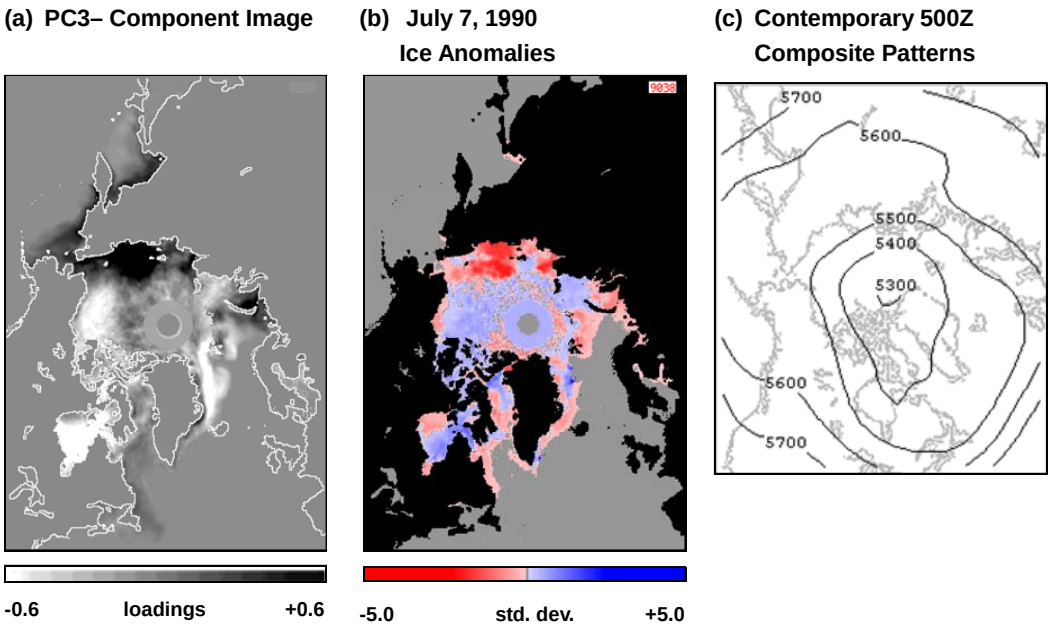

Figure 14. PC3– image and composite 500Z patterns.

pressure centre over the northern Canadian Archipelago in tandem with an Aleutian High. These were the atmospheric conditions present during prolonged ice anomaly periods in July 1990 and July 1992. The second sub-pattern also has a low pressure centre over the Canadian Archipelago (a bit further south than $PC3-_1$) as well as an elongated low in the vicinity of the Transpolar Drift Stream. Both sub-patterns are characterized by positive ice anomalies across the Arctic Basin, including Fram Strait and Hudson Bay, and lower ice concentrations in the East Siberian Sea.

4.4.3. PC3 Analysis

In a study of atmospheric circulation anomalies over the 1988 to 1995 period, Maslanik et al. (1996) found increased cyclone activity north of Siberia during April to September which led to a significant reduction in sea level pressure over the central Arctic Ocean and an increased flow of warm, southerly winds over the Eurasian sector. They observed reduced ice concentrations during this time and speculated that the warmer air had the effect of enhancing melt and reducing surface

albedo, promoting earlier break-up, and advecting the ice away from the Siberian coast towards the pole.

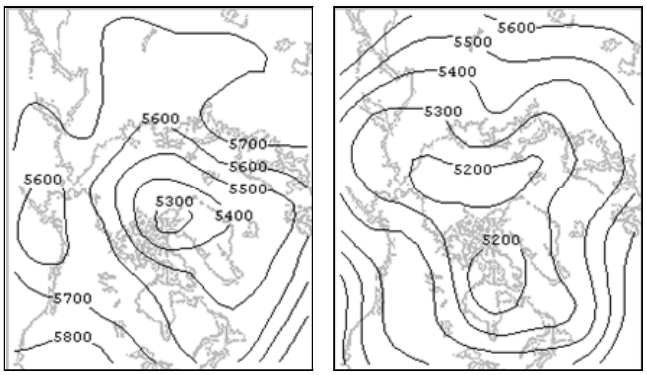

PC3–$_1$ Variance Explained: 72% Representativeness: 75%

PC3–$_2$ Variance Explained: 8% Representativeness: 25%

Figure 15. PC3– 500Z sub-patterns.

The observations made by Maslanik et al. (1996) fit well with the ice and atmospheric patterns identified in this component, particularly when it is in its negative mode. For example, the PC3 loadings (Figure 12) are relatively stable until about 1988, when their variance increases sharply. A review of the seasonality of the high PC3 loadings showed that the majority of the significant pentads – especially the negative pentads – occur between Day 17 (April 1) and Day 55 (September 30). The PC3– ice component and anomaly image (Figure 14b) is characterized by significantly reduced ice concentrations along the Siberian coast. Finally, the 500Z plot for PC3–$_2$ (Figure 15) shows a broad low pressure region over the central Arctic.

Maslanik et al. (1996) were hesitant to link these Arctic pressure anomalies with larger teleconnections and our analyses did not find any statistically significant lagged correlations between PC3 and any teleconnection time series.

4.5. Principal Component 4

The positive mode of Principal Component 4 (PC4) varies evenly across the time series but shows a marked swing from

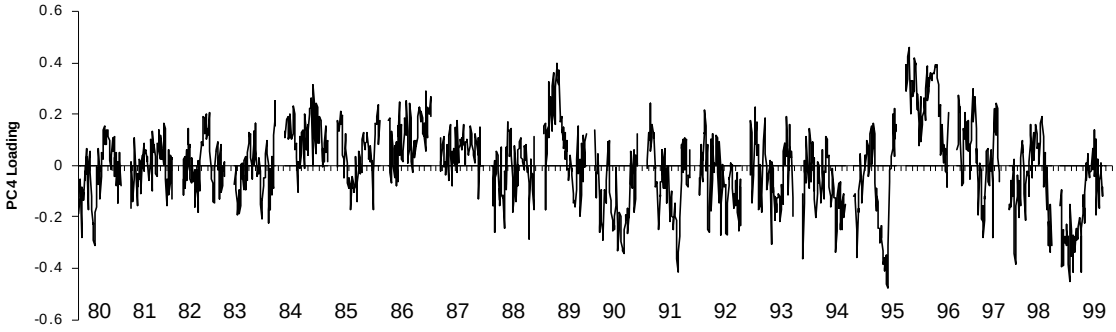

Figure 16. PC4 Loadings.

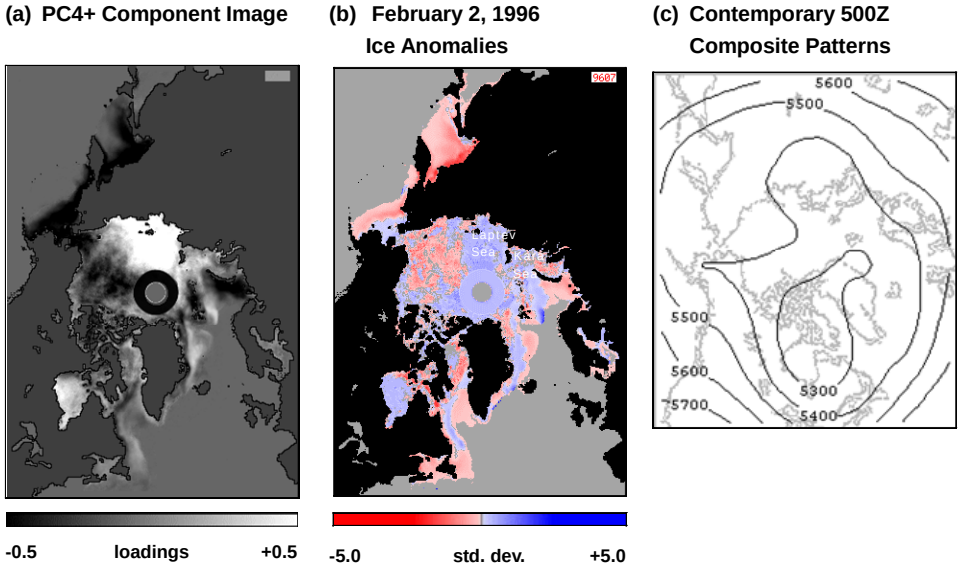

Figure 17. PC4+ image and composite 500Z patterns.

negative to positive modes in 1995 ~ 1996 (Figure 16). PC4+ was strongest late in the summers of 1980, 1984 and 1986, and during the spring months of 1989 an 1996, while there is no clear seasonality in the negative mode.

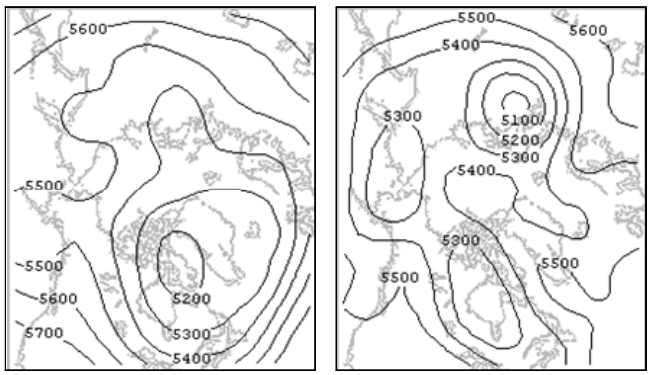

PC4+$_1$
Variance Explained: 50%
Representativeness: 75%

PC4+$_2$
Variance Explained: 26%
Representativeness: 25%

Figure 18. PC4+ 500Z sub-patterns.

4.5.1. PC4 Positive Mode

In its positive mode, PC4 is spatially associated with a strong region of positive loadings in the Laptev Sea, with weaker positive areas in the Greenland Sea and in Hudson Bay (Figure 17a). This pattern is exhibited quite well in the 9607 Pentad image in Figure 17b. The 500Z positive pattern composite image shows high pressure penetration over the Laptev and East Siberian Seas while the main centre of cyclonic activity is positioned over the eastern Canadian Archipelago (Figure 17c).

Figure 18 shows the results of the PCA decomposition of the atmospheric patterns that coincide with the positive phase of this ice component. The first atmospheric sub-pattern, PC4+$_1$ loads strongly for ice anomaly events throughout the time series, and is very similar to the group composite. The ridge over the East Siberian/Laptev seas is a consistent feature that seems relevant to the ice anomaly center in that region. The ice anomaly image shows generalized higher than average ice concentrations in the Kara and Laptev Seas. A positive ice anomaly also occurs in Hudson Bay along with negative anomalies in the Bering Sea.

The ice anomalies for PC4+$_2$ follow the same pattern as those for PC4+$_1$ although their atmospheric sub-patterns are each other. The atmospheric sub-pattern PC4+$_2$ is almost an inverse of PC4+$_1$; it loads strongly only for one ice anomaly event during April 1989, capturing a unique atmospheric pattern dissimilar to the group composite. The dominant low pressure center is shifted over Siberia and the Barents Sea and, while ridging penetrates the Arctic basin, it originates over the North Atlantic sector as opposed to the North Pacific.

4.5.2. PC4 Negative Mode

The negative mode for PC4 occurred during the summer months of 1990, 1991 and 1994, in the winters of 1980 and 1995, and over a protracted period during the fall of 1995. These periods are spatially associated with anomalous ice conditions in the Bering Sea and Sea of Okhotsk, and, to some extent, in the Beaufort Sea (Figure 19a). The centres of low pressure are very similar between the two modes of PC4, although in the PC4– mode there is a ridge of high pressure over the Beaufort Sea as opposed to the Laptev Sea (Figure 19c). There is only a weak

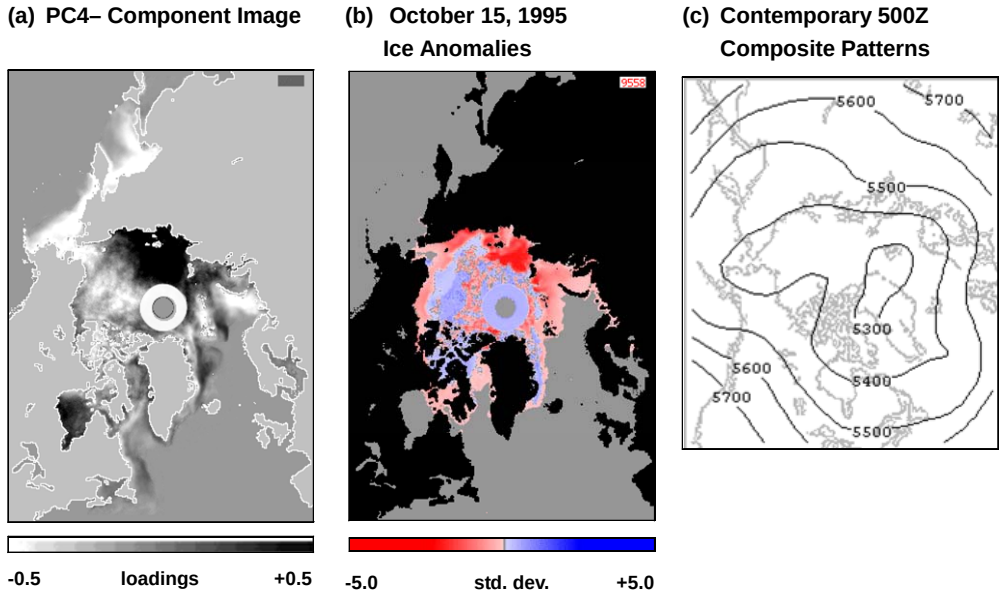

Figure 19. PC4– image and composite 500Z patterns.

match between the spatial patterns of the highest loading negative anomaly image in Figure 19b and the component image (Figure 19a). Caution should be used, therefore, in using the PC4– component image for any diagnostic or predictive purposes.

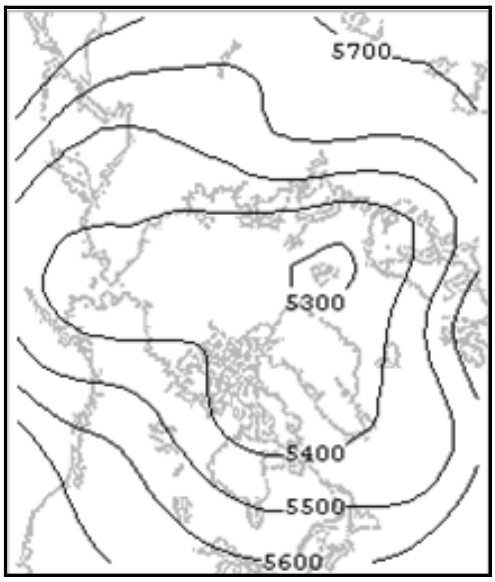

PC4–$_1$
Variance Explained: 69%
Representativeness: 92%

Figure 20. PC4– atmospheric sub-patterns.

The PC4– 500Z decomposition produced only a single significant sub-pattern (Figure 20). As expected, it is very similar to the group composite. The PC4–$_1$ sub-pattern characterizes inverse 500Z conditions over the Laptev Sea compared to 500Z components generated for ice anomaly PC4+ group, therefore results are clear and logical for this group. While PC4+ components characterize ridging over the ice anomaly center, this PC4– component illustrates the extension of an expansive, weak low pressure system over all of the Arctic Basin, extending over the ice anomaly center to the Bering Strait.

The ice concentration anomaly image shows generalized increased iciness over the North American side of the Arctic Ocean and strong, but localized, negative ice anomalies in the Eurasian side. This pattern is most representative of late summer/early fall conditions.

4.5.3. PC4 Analysis

The loadings in Figure 16 show a rapid shift from maximum negative mode (October 1995) to maximum positive mode (Feburary 1996). An examination of the individual anomaly images for these dates (not shown here) confirm the reversal of ice concentration conditions between the Laptev and Beaufort Seas. Interestingly, neither of these dates were identified as significant in the atmospheric analyses which raises some doubts about the strength of the ice-atmosphere relationship during the PC4 phase. A visual evaluation of the spatial patterns in the imagery presented above suggests that the PC4+$_2$ and PC4–$_1$ sub-patterns do correspond to the positive and negative modes of this ice anomaly, correspondingly. The PC4+$_1$ sub-pattern does not correspond well with any of the other spatial patterns so we question its validity with this ice component.

Spatially, there seems to be higher than average ice concentrations on the Eurasian side of the Arctic Basin during PC4+ periods and greater positive ice anomalies on the North American side in PC4– mode. This spatial-termporal pattern was evident in our previous analysis of the SMMR series (Piwowar and LeDrew, 1996), but not at all in the SSM/I analysis (Piwowar et al., 1996).

A similar variability has been described by Walsh and Johnson (1980b) and Gloersen et al. (1993). Gloersen et al. (1993) refer to the North American tendency as the "Alaskan mode" and the Eurasian position as the "Siberian mode". They describe the Alaskan mode as causing positive ice concentration anomalies along the Beaufort Sea coastline as the ice impinges upon the shore. In the Siberian mode a wide band of open water appears along the Beaufort Sea coastline resulting in negative concentration anomalies as the ice is displaced towards the Eurasian continent. Both of these modes are well illustrated by the ice concentration anomaly images in Figure 17 and Figure 19.

Gloersen et al. (1993) suggest that the position of the summer ice pack is closely linked to the principal ice drift patterns in the Arctic Basin. They propose that during years when the drift streams are well established the ice is carried away from the Beaufort Sea coast by the Beaufort Sea Gyre and delivered into the Transpolar Drift Stream, where it is ferried along towards Fram Strait. These are the years of the Siberian mode. When the Alaskan mode occurs, there is very little ice movement along these established tracks.

This analysis is supported by Kwok (2000) who links the Arctic Basin drift patterns with the North Atlantic Oscillation. He found that during NAO– years the Transpolar Drift Stream is strong and runs parallel to the Siberian coast. This characteristic is captured in the PC4+ ice concentration anomaly image in Figure 17b. Notice the positive anomalies originating along the Siberian coast and running through the Arctic Ocean toward Fram Strait – the path taken by the Transpolar Drift Stream. During NAO+ periods, Kwok (2000) found the Transpolar Drift Stream to be much weaker and shifted towards the Canadian Basin. This pattern is evident in the PC4– anomaly image in Figure 19b.

Visually, the PC4 loadings in Figure 16 appear to mirror the NAO pattern. Between 1980 and 1987, the NAO frequently moved from one mode to the other and there were about the same number of NOA+ and NAO– periods (Kwok, 2000). The PC4 loadings are generally clustered around 0, with few outliers. In 1988, the NAO entered a prolonged positive phase that lasted until 1995. In 1988, the PC4 loadings become predominantly negative and remained that way until 1995. The NAO+ mode ended with a "dramatic reversal in phase in 1996" (Kwok, 2000). We see a similar dramatic shift in the PC4 load-

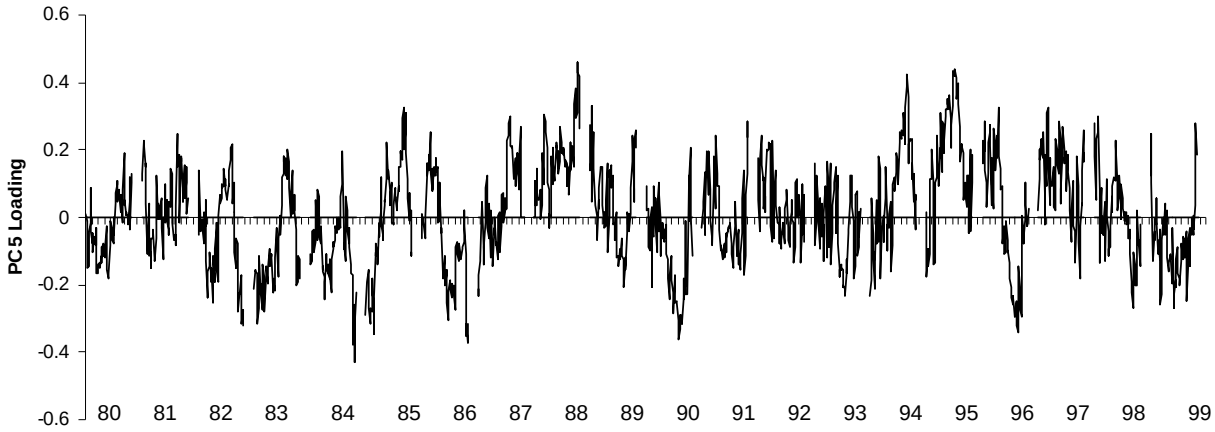

Figure 21. PC5 Loadings.

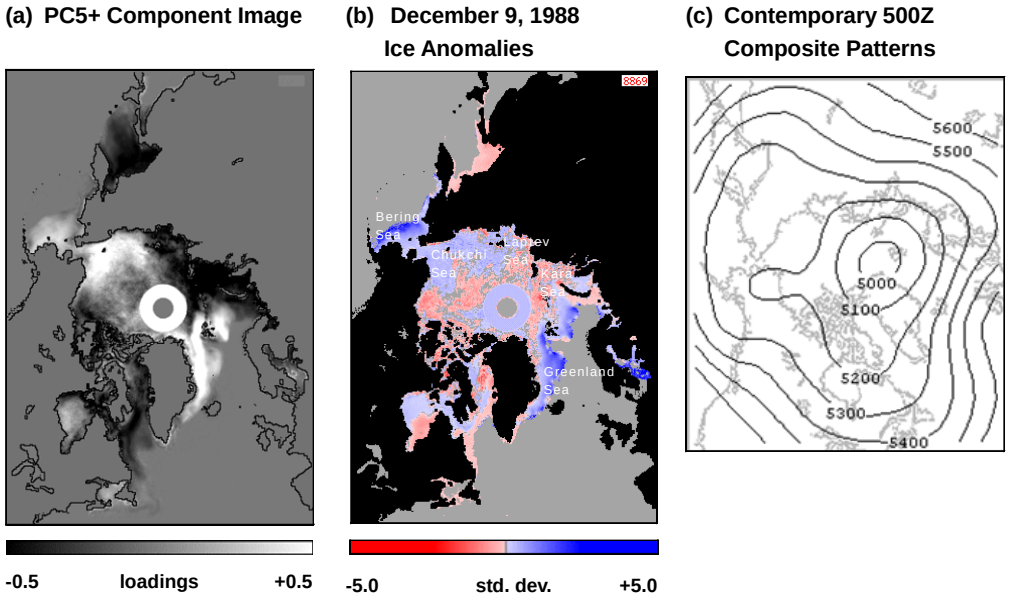

Figure 22. PC5+ image and composite 500Z patterns.

ings between 1995 and 1996.

Thus, PC4 appears to be related to the NAO, with the positive NAO phase contemporary with the "Alaskan mode" and PC4– and the NAO– phase associated with the "Siberian mode" and PC4+. We did not find any statistically significant lagged correlations between PC4 and any teleconnection time series, however.

4.6. Principal Component 5

The loadings for the fifth principal component are presented in Figure 21. Temporally, they appear to oscillate on a 1 to 2 year cycle. The positive mode dominated in 1985, 1988 and 1995, all during the fall. The negative mode was strongest during the autumns of 1980, 1982, 1984, 1986, 1990 and 1996. The highest positive loading occurred during a long positive period centered on December 9, 1988. This image is shown in Figure 22b, below. The image in Figure 24b shows the ice anomalies for the lowest negative loading on December 19, 1984.

4.6.1. PC5 Positive Mode

Principal Component 5 spatially shows in-phase anomalies between the eastern and western outlets of the Arctic Ocean (Figure 22a). There is a good spatial correspondence between the anomaly image in (Figure 22b) and the PC5 component image, thereby validating this component. In the PC5 positive mode (PC5+), there are strong positive ice anomalies in the Bering, Chukchi and Greenland Seas. Atmospherically, cyclonic activity is centered over Fram Strait in the positive mode (Figure 22c). The low pressure cell is more localized for PC5+ than for PC5–. and over Baffin Island in the negative

phase.

All contemporary 500Z pentads load the most strongly to the first sub-pattern ($PC5+_1$), indicating a strong degree of spatial similarity in the 500Z fields related to the positive phase of ice anomaly PC5 (Figure 23). On the $PC5+_1$ pressure map in we see a concentric low pressure centre over the Eastern Arctic Ocean where it drains through Fram Strait.

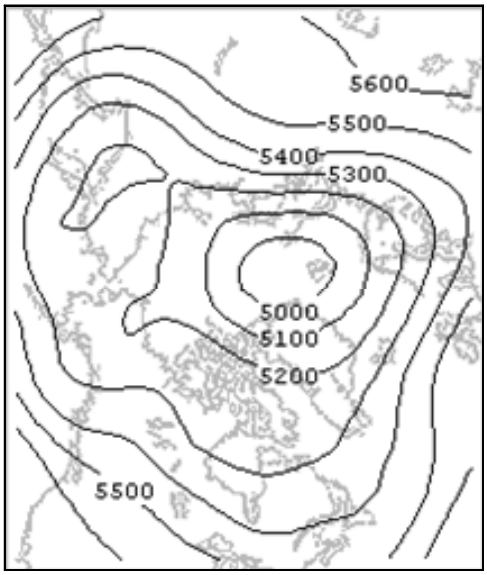

PC5+$_1$
Variance Explained: 77%
Representativeness: 100%

Figure 23. PC5+ 500Z sub-pattern.

4.6.2. PC5 Negative Mode

The negative mode of PC5 is associated with positive ice concentration anomalies in the Sea of Okhotsk, the Barents Sea, the Canadian Archipelago, and through Davis Strait (Figure 24a, b). The negative mode depicts ridging over the Greenland Sea that is not apparent in the positive phase (Figure 24c).

Just as with the PC5+ group, the first PC5– 500Z sub-pattern is dominant so the atmospheric patterns closely match those of the group composite (Figure 25). In we see an expansive area of generally low pressure over the Arctic Basin, with deeper centres over Baffin Island and the Chukchi Sea. Some ridging is evident over the Greenland Sea; there may be an important connection between this ridging and the ice anomalies highlighted there.

4.6.3. Analysis

All the significant loadings for PC5 occur in the fall and correspond to in-phase ice anomalies in the Chukchi and Greenland Seas and a phase-shifted anomaly in the Kara and Laptev Seas. This anomaly pattern oscillates between negative and positive modes in an inter-annual cycle lasting between 1 and 2 years. The significant anomalies are distributed evenly across the time series and are not concentrated at during any particular period. This would suggest that the forcing mechanisms for this anomaly pattern are episodic in nature, rather than related to low frequency atmospheric or oceanic fluctuations.

Given that the atmospheric sub-pattern anomaly images have a good spatial correspondence with the PC5 component image, we can say that the 500Z composites given in Figure 22c and Figure 24c accurately represents the atmospheric con-

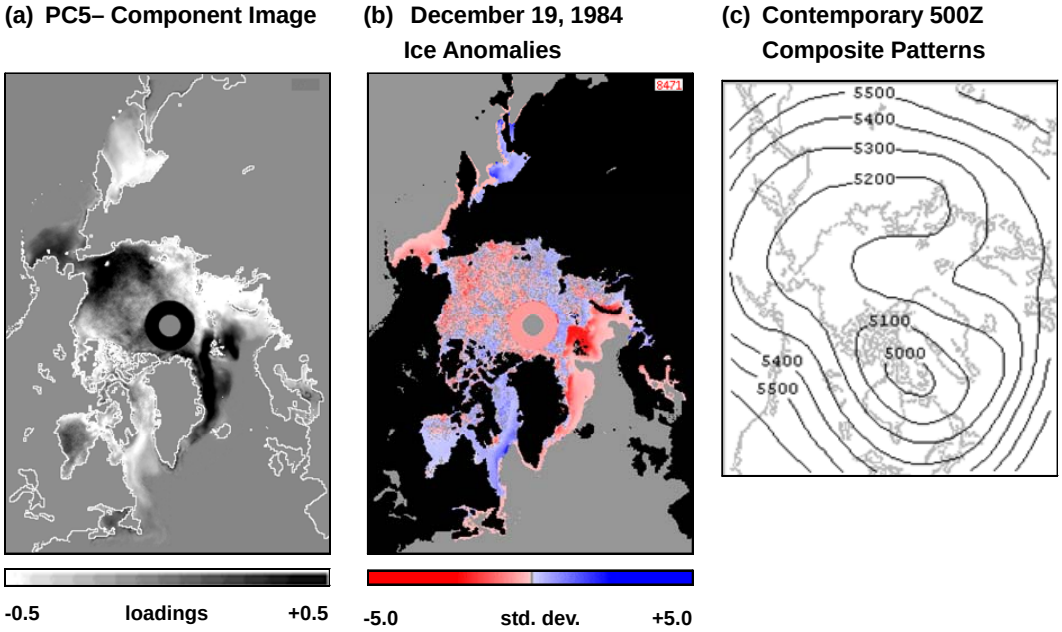

Figure 24. PC5– image and composite 500Z patterns.

ditions present during these anomaly events. During the PC5 positive mode there may be atmospheric forcing of ice out of the Kara and Laptev Seas and into the East Siberian and Kara Seas. The increased concentrations here may feed into the Transpolar Drift Stream where its is exported into the Greenland Sea. During PC5 negative mode conditions, the shift of the low pressure centre away from Fram Strait and over Baffin Island may cuase divergence from Fram Strait.

We did not find any statistically significant lagged correlations between PC5 and any teleconnection time series.

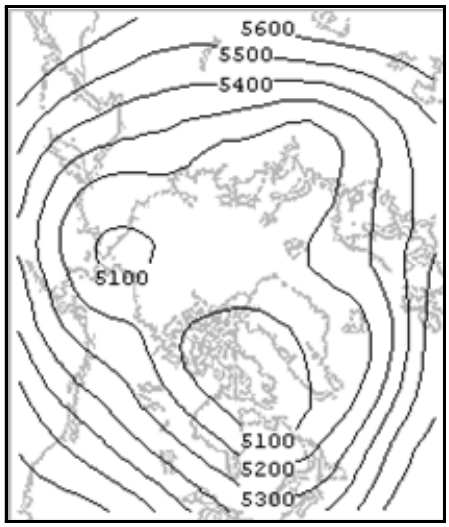

PC5–$_1$
Variance Explained: 74%
Representativeness: 100%

Figure 25. PC5– 500Z sub-patterns

5. Discussion

During the preceding principal components analysis of sea ice concentration anomalies, it became clear that it was not only the component images which bore important information, but the loadings plots also had the potential to reveal meaningful insights. For example, in each loadings time series there is a distinct change in the character of the data starting in the period between 1987 and 1990. For each component this change is unique and typically lasts for three or more years. These changes are summarized in Table 1.

We suggest several possible explanations for these changes:

1) The observed patterns may be due to a decadal shift in the ice concentration patterns. Ikeda (1990a, b) and Barry et al. (1993) noted that some areas of the Arctic ice pack appear to follow decadal-scale oscillations. Other researchers have suggested that various components of the cryospheric system also follow a decadal pattern (e.g. Mysak and Manak, 1989; Coughlan and Nyenzi, 1990; Brown and Cote, 1992; Kerr, 1992). Although our observations appear to be congruent with these theories, a time series spanning just twenty years is too short to detect decadal scale patterns with confidence.

2) The change in the timing of ice concentration anomalies may be mirroring the influence of changing atmospheric systems over the north polar region. In a study of atmospheric circulation anomalies over the 1988 ~ 1995 period, Maslanik et al. (1996) found increased cyclone activity north of Siberia during April to September which led to a significant reduction in sea level pressure over the central Arctic Ocean and an increased flow of warm, southerly winds over the Eurasian sector. They observed reduced ice concentrations during this time and speculated that the warmer air had the effect of enhancing melt and reducing surface albedo, promoting earlier break-up, and advecting the ice away from the Siberian coast towards the pole.

3) The shift from negative to positive modes near 1987 may be related to the change in sensor data used for the time series. For the period January 1980 to July 1987 SMMR data were used while the SSM/I operated from July 1980 on. Although the ice concentrations were adjusted to improve inter-sensor consistency (Cavalieri et al., 1999), Derksen and Walker (2003) suggest that adjustment factors are not globally applicable; rather the region and application must be considered. Such changes, if present, would be highlighted by the PCA and could be the pattern observed here.

4) The mode change from a period of generally positive ice anomalies to one of negative anomalies (e.g. PC2) and an increase in variability (e.g. PC3) may be indicative of a true climatic shift in this region. We know that the 1990s period was the warmest decade on instrumental record (Karl et al., 2000) and this may be reflected in the polar ice. This theory is supported by the fact that PC2 has the strongest loadings in the spring and fall transition periods, and the timing and rates of sea ice growth and decay may be one of the more sensitive indicators of general climatic conditions.

Each of the above explanations is plausible, but none fit all the data all of the time. It is most likely that each factor contributes some portion of influence to the whole. Ultimately, however, we believe that these temporal observations have the strongest association with the North Atlantic Oscillation and other global teleconnections. For example, the NAO was persistently positive between 1989 and 1996 and there was an extended ENSO event between 1990 and 1995. Parkinson et al. (1999) link the unusually heavy ice coverages in Hudson and Baffin Bays, and in the Labrador Sea in 1982-83 and 1991-92 with strong and simultaneous NAO and ENSO episodes. In the present analysis, we found statistically significant correlations between the entire PC1 time series and the NAO and AO and noted that a strong NAO was typically coincident with PC1, PC4 and PC5 peak periods.

6. Summary and Conclusions

In this research our analysis approach has been to find the temporally/spatially strongest recurring ice anomaly patterns and then identify contemporary atmospheric pentads. Our intention was to provide observational evidence for the link-

Table 1. Changes in Temporal Characteristics of PC Loadings

Ice Anomaly Component	Period of Change	Characteristics of Change
PC 1	1988 - 1995	prolonged negative mode; this follows a consistently oscillating period
PC 2	1987 - end	shift from predominately negative mode to predominately positive mode
PC 3	1988 - end	sharp increase in variability
PC 4	1989 - 1995	predominately negative phase; terminated by a sharp shift into positive mode
PC 5	1990 - 1994	reduced variability

ages between the ice and the global atmospheric system, rather than to identify cause and affect relationships. Using Principal Components Analysis, we have captured the five largest temporally repeating ice concentration anomaly patterns in the Northern Hemisphere and have identified their contemporary 500Z pressure patterns.

The strongest spatial-temporal ice concentration anomaly pattern over the 1980 to 1999 period was the phase-shifted anomalies between the Greenland and Barents Seas and the Labrador Sea and in Davis Strait. The strongest loadings to this component were between 1983 and 1984 and from 1990 to 1993 when there were negative ice concentration anomalies east of Greenland and much higher than average ice concentrations closer to North America (PC1− mode). This was also the highest component found by Slonosky et al. (1997) when they analyzed the Walsh and Chapman ice anomaly data set from 1954 to 1990. We found this pattern to be associated with strong low pressure anomalies over the North Atlantic and is significantly correlated with the large-scale atmospheric patterns of the NAO and El Niño.

The Beaufort Sea is another region where a consistent pattern of decreased ice concentrations was identified. This mode (PC2+) has been generally positive since 1988, particularly in the summer months. The associated 500Z pattern shows a typical warm season central polar low with a weak 500Z latitudinal gradient. This component is probably highlighting the anomaly pattern associated with the quasi-annual reversal of the Beaufort Sea Gyre.

Negative ice concentration anomalies on the Siberian side of the Arctic were also identified as spatially and temporally strong (PC3–). We showed these anomalies to be coincident with low pressure centered over the northern Canadian Archipelago in tandem with an Aleutian High which could produce an increased flow of warm, southerly winds over the Siberian sector.

The fourth principal component (PC4–) appears to be related to the general oscillation of the Arctic ice pack between the North American and Eurasian sides of the Arctic basin. We found the shifting phases in the ice to be coincident with alternating 500Z pressure modes over the Laptev Sea. The loadings time series for this component are visually similar to the NAO index, although a statistically significant correlation was not found. We did find an association of the timing of the PC4+ pentads with the NAO and El Niño series, however.

All the significant loadings for fifth component (PC5) occur in the fall and correspond to in-phase ice anomalies in the Chukchi and Greenland Seas and a phase-shifted anomaly in the Kara and Laptev Seas. Generally, these ice anomalies are associated with an expansive area of low pressure over the Arctic Basin with a centre that oscillates between the eastern Arctic Ocean and Baffin Island. The significant anomalies are distributed evenly across the time series and are not concentrated at during any particular period. This would suggest that the forcing mechanisms for this anomaly pattern are episodic in nature, rather than related to low frequency atmospheric or oceanic fluctuations.

In this work, we have primarily examined co-occurring ice and atmospheric patterns. We found a statistically significant relationship between the NOA and PC1 and a plausible relationship between the NAO and PC4. This provides further evidence of the NAO as a dominant mechanism controlling Arctic sea ice. Even though PC1 was the only component studied that had statistically significant correlations with low-frequency atmospheric teleconnection patterns, we found weak correlations with all of the components. Although these coincidences do not necessarily imply teleconnectivity, they should be explored further to determine if more formal relationships can be established. We know from our work herein and elsewhere (e.g. Slonosky et al., 1997), however, that there may be stronger time lagged correlations between the ice and the atmosphere. A more detailed look at the lagged relationships between the atmospheric components and the ice anomalies could reveal more significant relationships than those uncovered here. This will be the subject of future communications.

Principal components analysis has been shown to be a very useful tool for identifying spatial patterns of sea ice concentrations and atmospheric pressures that occurred at various times in twenty-year period. The strength of this approach, over other hypertemporal procedures, is that it can isolate significant variations in the data both spatially *and* temporally. The component images show the spatial arrangement of a particular ice concentration pattern while the loadings plots show when in the time series it is most prevalent.

The analyses reported here provide a benchmark of sea ice-atmospheric teleconnections for the two decades leading up to 2000. Since then, the Arctic ice cover has continued to recede and in 2002 the Northern Hemisphere ice cover reached a record minimum (Serreze et al., 2003; Stroeve et al., 2005), and is receiving considerable international attention (e.g., IPCC, 2007; Serreze et al., 2007). Because the Arctic is so integrally connected with the Earth's climate system, there is concern that the recent changes in sea ice cover may have reached a tipping point that could trigger a cascade of global changes (Serreze et al., 2007). The interdecadal climatologies

developed here are fundamental for the continued monitoring of polar condi- tions.

Acknowledgments. This research was funded by Environment Canada through the CRYSYS research initiative.

References

Barnston, A. and Livezey, R. (1987). Classification, seasonality and persistence of low-frequency atmospheric circulation patterns, *Mon. Weather Rev.*, 115, 1083-1126, doi:10.1175/1520-0493(1987)115<1083:CSAPOL>2.0.CO;2.

Barry, R.G., Maslanik, J., Steffen, K., Weaver, R.L., Triosi, V., Cavallier, D.J. and Martin, S. (1993). Advances in sea-ice research based on remotely sensed passive microwave data, *Oceanography*, 6(1), 5-13.

Bond, N. and Harrison, D. (2000). The Pacific Decadel Oscillation, air-sea interaction and central north Pacific winter atmospheric regimes, *Geophys. Res. Lett.*, 27(5), 731-734.

Brown, R.D. and Cote, P. (1992). Interannual variability of landfast ice thickness in the Canadian High Arctic, (1950-89). *Arctic*, 45 (3), 273-284.

Cavalieri, D.J., Parkiinson, C.L., Gloersen, P., Comiso, J.C. and Zwally, H.J. (1999). Deriving long-term time series of sea ice cover from satellite passive-microswave multisensor data sets, *J. Geophys. Res.*, 104, 15803-15814, doi:10.1029/1999JC900081.

Colony, R. and Thorndike, A.S. (1984). An estimate of the mean field of Arctic sea ice motion, *J. Geophys. Res.*, 89(C6), 10623-10629.

Comiso, J.C., Cavalieri, D., Parkinson C. and Gloersen, P. (1997). Passive microwave algorithms for sea ice concentrations: A comparison of two techniques, *Remote Sens. Environ.*, 60(3), 357-384, doi:10.1016/S0034-4257(96)00220-9.

Coppin, P., Jonckheere, I., Nackaerts, K. and Muys, B. (2004). Digital change detection methods in ecosystem monitoring: A review, *Int. J. Remote Sens.*, 25(9), 1565-1596, doi:10.1080/01431160310001016757 5.

Coughlan, M.J. and Nyenzi, B.S. (1990). Climate trends and variability. Climate change: Science, impacts and policy, in *Proc. of the 2nd World Climate Conference*, Cambridge University Press, Cambridge, pp. 71-82.

Derksen, C., LeDrew, E., Walker, A. and Goodison, B. (2000). Winter season variability in North American Prairie SWE distribution and atmospheric circulation, *Hydrol. Process.*, 14(18), 3273-3290, doi:10.1002/1099-1085(20001230)14:18<3273::AID-HYP203>3.0.CO;2-W.

Derksen, C. and Walker, A.E. (2003). Identification of systematic bias in the cross-platform (SMMR and SSM/I) EASE-Grid brightness temperature time series, *IEEE Trans. Geosci. Remote Sens.*, 41(4), 910-915, doi:10.1109/TGRS.2003.812003.

Deser, C. (2000). On the teleconnectivity of the "Arctic Oscillation", *Geophys. Rese. Lett.*, 27(6), 779-782.

Eastman, J.R. and Fulk, M. (1993). Long sequence time series evaluation using standardized principal components, *Photogramm. Eng. Remote Sensing*, 59(8), 1307-1312.

Fung, T. and LeDrew, E. (1987). Application of principal components analysis to change detection, *Photogramm. Eng. Remote Sensing*, 53(12), 1649-1658.

Gloersen, P., Campbell, W.J., Cavalieri, D.J., Comiso, J.C., Parkinson, C.L. and Zwally, H.J. (1993). Arctic and Antarctic Sea Ice, (1980- 1987): Satellite Passive-Microwave Observations and Analysis, National Aeronautics and Space Administration, NASA SP-511, Washington DC.

Holt, B. and Martin, S. (2001). The effect of a storm on the 1992 summer sea ice cover in the Beaufort, Chukchi, and East Siberian Sea,. *J. Geophys. Res.*, 106, 1017-1032, doi:10.1029/1999JC000110.

Ikeda, M. (1990a). Feedback mechanism among decadal oscillations in Northern Hemisphere atmospheric circulation, sea ice, and ocean circulation, *Ann. Glaciol.*, 14, 120-123.

Ikeda, M. (1990b). Decadal oscillations of the air-ice-ocean system in the Northern Hemisphere, *Atmosphere-Ocean*, 28(1), 106-139.

IPCC (2001). *Climate Change 2001: Synthesis Report*, *Third Assessment Report of the Intergovernmental Panel on Climate Change*, Cambridge University Press, Cambridge.

IPCC (2007). *Climate Change 2007: Impacts, Adaptation and Vulnerability, Working Group II Contribution to the Inter-governmental Panel on Climate Change Fourth Assessment Report*, IPCC Secretariat, Geneva.

Jenne, R. (1970). *The NMC Octagonal Grid*, National Center for Atmospheric Research Technical Note.

Jensen, J.R. (1986). *Introductory Digital Image Processing: A Remote Sensing Perspective*, Prentice-Hall, Englewood Cliffs, NJ,

Karl, T., Knight, R. and Baker, B. (2000). The record breaking global temperatures of 1997 and 1998: Evidence for an increase in the rate of global warming? *Geophys. Res. Lett.*, 27(5), 719-722, doi:10.1029/1999GL010877.

Kelly, P.M., Jones, P.D., Sear, C.B., Cherry B.S.G. and Tavakol, R.K. (1982). Variations in surface air temperatures: Part 2. Arctic Regions, 1881-1980. *Mon. Weather Rev.*, 110, 71-83, doi:10.1175/1520-0493(1982)110<0071:VISATP>2.0.CO;2.

Kerr, R.A. (1992). Unmasking a shifty climate system, *Sci.*, 255, 1508-1510, doi:10.1126/science.255.5051.1508.

Kutzbach, J.E. (1967). Empirical eigenvectors of sea-level pressure, surface temperature and precipitation complexes over North America, *J. Appl. Meteorol.*, 6, 791-802, doi:10.1175/1520-0450(1967)006<0791:EEOSLP>2.0.CO;2.

Kwok, R. (2000). Recent changes in Arctic Ocean sea ice motion associated with the North Atlantic Oscillation, *Geophys. Res. Lett.*, 27(6), 775-778, doi:10.1029/1999GL002382.

LeDrew, E.F., Johnson, D. and Maslanik, J.A. (1991). An examination of atmospheric mechanisms that may be responsible for the annual reversal of the Beaufort sea ice field, *Int. J. Climatol.*, 11, 841-859

Lillesand, T.M. and Kiefer, R.W. (2000). *Remote Sensing and Image Interpretation (4th Edition)*, John Wiley & Sons, New York.

Mantua, N.J., Hare, S.R., Zhang, Y., Wallace, J.M. and Francis, R.C. (1997). A Pacific interdecadal climate oscillation with impacts on salmon production, *Bull. Am. Meteorol. Soc.*, 78, 1069-1079, doi:10.1175/1520-0477(1997)078<1069:APICOW>2.0.CO;2.

Maslanik, J.A., Serreze, M.C. and Barry, R.G. (1996). Recent decreases in Arctic summer ice cover and linkages to atmospheric circulation anomalies, *Geophys. Res. Lett.*, 23(13), 1677-1680, doi:10.1029/96GL01426.

Millward, A.A., Piwowar, J.M. and Howarth, P.J. (2006). Change analysis using a time series of multi-sensor data, *Photogramm. Eng. Remote Sensing*, 72(6), 653-664.

Mysak, L.A. and Manak, D.K. (1989). Arctic sea-ice extent and anomalies, (1953-1984), *Atmosphere-Ocean*, 27(2), 376-405.

NRC (2000). *Reconciling Observations of Global Temperature Change, Panel on Reconciling Temperature Observations*, Climate Research Committee, National Research Council, Academic Press, Washington DC.

NSIDC (2000). Bootstrap Sea ice Concentrations from Nimbus-7 SMMR and DMSP SSM/I. http://nsidc.org/ NASA/GUIDE/docs/dataset_documents/bootstrap_time_series_dataset_docment.html.

Parkinson, C.L. and Cavalieri, D.J. (1989). Arctic sea ice (1973-1987): Seasonal, regional, and interannual variability, *J. Geo-*

phys. Res., 94(C10), 14499-14523.

Parkinson, C.L., Cavalieri, D.J., Gloersen, P., Zwally, H.J. and Comiso, J.C. (1999). Arctic sea ice extents, areas, and trends, (1980-1996), *J. Geophys. Res.*, 104, 20837-20856, doi:10.1029/1999JC900082.

Piwowar, J.M. and LeDrew, E.F. (1995). Hypertemporal analysis of remotely sensed sea-ice data for climate change studies, *Prog. Phys. Geogr.*, 19(2), 216-242, doi:10.1177/030913339501900204.

Piwowar, J.M. and LeDrew, E.F. (1996). Principal components analysis of Arctic ice conditions between 1980 and 1987 as observed from the SMMR data record, *Can. J. Remote Sens.*, 22(4), 390-403.

Piwowar, J.M., Peddle, D.R. and LeDrew, E.F. (1997). Temporal mixture analysis of Arctic sea ice imagery: A new approach for monitoring environmental change, *Remote Sens. Environ.*, 63, 195-207, doi:10.1016/S0034-4257(97)00105-3.

Piwowar, J.M. and LeDrew, E.F. (2002). ARMA time series modelling of remote sensing imagery: A new approach for climate change studies, *Int. J. Remote Sens.*, 23(24), 5225-5248, doi:10.1080/01431160110109552.

Roads, J., Chen, S. and Ueyoshi, K. (1995). Comparison of NMC's global pressure analysis to NCDC's US observations, *J. Clim.*, 8, 1410-1428.

Sellers, W.D. (1968). Climatology of monthly precipitation patterns in the Western United States, 1931-1966. *Mon. Weather Rev.*, 96(9), 585-595, doi:10.1175/1520-0493(1968)096<0585:COMPPI>2.0.CO;2.

Serreze, M.C., Maslanik, J.A., Scambos, T.A., Fetterer, F., Stroeve, J., Knowles, K., Fowler, C., Drobot, S., Barry, R.G. and Haran, T.M. (2003). A record minimum Arctic sea ice extent and area in 2002, *Geophys. Res. Lett.*, 30(3), 1-4, doi:10.1029/2002GL016406.

Serreze, M.C., Holland, M.M. and Stroeve, J. (2007). Perspectives on the Arctic's shrinking sea-ice cover, *Sci.*, 315(5818), 1533-1536, doi:10.1126/science.1139426.

Slonosky, V.C., Mysak, L.C. and Derome, J. (1997). Linking Arctic sea-ice and atmospheric circulation anomalies on interannual and decadal timescales, *Atmosphere-Ocean*, 35(3), 333-366.

Stroeve, J.C., Serreze, M.C., Fetterer, F., Arbetter, T., Meier, W., Maslanik, J. and Knowles, K. (2005). Tracking the Arctic's shrinking ice cover: Another extreme minimum in 2004, *Geophys. Res. Lett.*, 32(4), L04501, doi:10.1029/2004GL021810.

Trenberth, K. and Olson, J. (1988). An evaluation and inter-comparison of global analysis from the National Meteorological Center and the European Centre for Medium Range Weather Forecasts, *Bull. Am. Meteorol. Soc.*, 69(9), 1047-1057, doi:10.1175/1520-0477(1988)069<1047:AEAIOG>2.0.CO;2.

Wallace, J. and Gutzler, D. (1981). Teleconnections in the potential height field during the Northern Hemisphere winter, *Mon. Weather Rev.*, 109, 784-812.

Walsh, J.E. and Johnson. C.E. (1980). An analysis of Arctic sea ice fluctuations, 1953-77, *J. Phys. Oceanography*, 9, 580-591, doi:10.1175/1520-0485(1979)009<0580:AAOASI>2.0.CO;2.

Wilkinson, L. (1989). *SYSTAT: The System for Statistics*, SYSTAT, Evanston, IL.

Zhang, Y., Wallace, J.M. and Battisti, D.S. (1997). ENSO-like interdecadal variability: 1900-93, *J. Clim.*, 10, 1004-1020.